Magnetostatic wave dynamic magnetization response in yttrium iron garnet films

Mincho A. Tsankov,[a] Ming Chen, and Carl E. Patton[b]
Department of Physics, Colorado State University, Fort Collins, Colorado 80523

(Received 15 February 1995; accepted for publication 23 October 1995)

The dynamic microwave magnetization (DMM) amplitude of magnetostatic waves in yttrium iron garnet films at 5–6 GHz has been measured as a function of input power. The measurement is based on the characteristic frequency shift in the power transmission spectrum. This shift is related to the reduction of the effective static magnetization and, therefore, the increase of the DMM amplitude at high power. The measurements were made on 7.2-μm-thick, single-crystal yttrium iron garnet films. A pulsed frequency-swept microwave signal at 5–6 GHz was used to launch the magnetostatic waves. The signals were excited and detected by planar microstrip transducers. Measurements were made for magnetostatic forward volume waves (MSFVW) and magnetostatic surface waves (MSSW). The duty cycle of the pulsed microwave signal was kept at 0.1% in order to avoid sample heating effects. The shifts for small features in the transmission vs frequency profiles were used to determine the DMM amplitudes. At low power, the DMM amplitude increased with power. Saturation occurred at high power. The results indicate a saturation DMM response at about 10% of the saturation magnetization for input power in the 3–4 W range for MSFVW signals and above 0.5 W for MSSW signals. © *1996 American Institute of Physics.* [S0021-8979(96)05703-1]

I. INTRODUCTION

The amplitude of the dynamic microwave magnetization is an important parameter for studies of nonlinear magnetostatic wave (MSW) phenomena in yttrium iron garnet (YIG) films at high power. This amplitude, for example, has been a key factor in recent work on microwave magnetic envelope solitons.[1–6] In Refs. 3–6, for example, estimates of the dynamic microwave magnetization (DMM) amplitude response as a function of input power were needed in order to compare experimental data on magnetostatic wave solitons with the numerical modeling results obtained from the nonlinear Schrödinger equation.

Direct calibration of the DMM amplitude as a function of input power is difficult because of the many factors affecting the efficiency of the microstrip transducers used to excite the MSW signals, the problem of significant MSW signal decay during propagation, and saturation effects due to nonlinear processes. Accordingly, calculations of the DMM amplitude with the aid of linear MSW theory[7] provide only a rough estimate of the actual response at high power levels.[8] Estimates of the uniform mode magnetization precession angle in ferromagnetic resonance experiments in YIG films have been obtained from Faraday rotation measurements.[9]

The DMM amplitude of magnetostatic wave signals at high power levels should affect the high frequency magnetic response in a very simple way, through shifts in the MSW transmission vs frequency profiles. This article describes such measurements, based on the reduction of the static component of the film magnetization which occurs when the DMM amplitude increases. This reduction gives rise to a characteristic frequency shift of the MSW transmission loss frequency profile. If this profile is measured as a function of input power, the DMM amplitude may be obtained directly from the measured frequency shift.

This technique has been applied to two specific MSW configurations, magnetostatic forward volume wave (MSFVW) excitations and magnetostatic surface wave (MSSW) excitations, in a 7.2-μm-thick YIG film sample in a standard microstrip delay line structure. The measurements were made at 5–6 GHz. Conventional network analyzer measurements of transmission profiles of output power vs frequency over the entire MSW pass band were first made at low power. Selected features on these profiles were identified. Then, the network analyzer was operated in a pulsed mode at a very low duty cycle to remeasure profile segments containing these features and determine frequency shifts for the selected features as a function of power. These shifts were then related to the DMM amplitude on the basis of nonlinear FMR response theory. The DMM amplitude was found to scale with the input power at low power levels, typically below 0.1–0.5 W or so. This response is consistent with results from microwave pulse soliton measurements with similar transducer structures. A saturation in the DMM amplitude was found at higher input powers, and the saturation amplitude was about 10% of the YIG static magnetization.

II. FREQUENCY SHIFT WITH POWER

This section considers the formal analysis of the microwave magnetic excitations associated with MSFVW and MSSW signals in YIG films and develops the quantitative connections between the DMM amplitude and frequency shift of the MSFVW and MSSW transmission loss curves at high power. The analysis is based on a classical precession model for the magnetization in a saturated thin film and unidirectional in-plane propagation of the associated excitation.

[a]Present address: Sierra Microwave Technology, One Sierra Way, Georgetown, TX 78626.
[b]Electronic mail: patton@lamar.colostate.edu

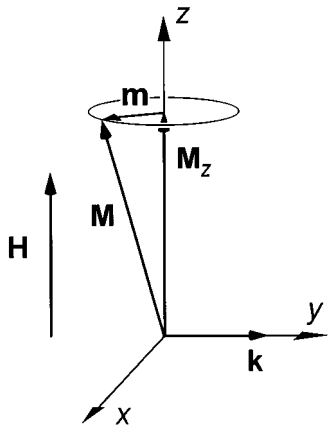

FIG. 1. Diagram of the magnetization field precession geometry. The static internal field **H** is along the z direction. The magnetization vector **M** precesses about this field with a dynamic magnetization **m** in the $x-y$ plane and a z directed static magnetization component M_z. The wave vector **k** in the y direction denotes the magnetostatic wave propagation direction.

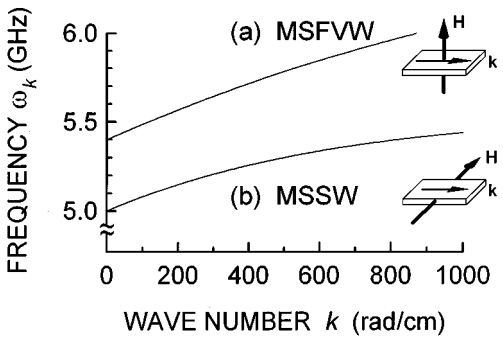

FIG. 2. Dispersion diagrams of frequency ω_k vs wave number k for (a) magnetostatic forward volume wave (MSFVW) and (b) magnetostatic surface wave (MSSW) signals in a YIG film, along with applicable film orientation diagrams. Curve (a) is for a perpendicular-to-film internal magnetic field $H=1929$ Oe and curve (b) is for an in-plane internal magnetic field $H=1114$ Oe.

Decay in the precession amplitude during propagation due to relaxation and nonclassical nonlinear processes are ignored.

Figure 1 shows the magnetization and field geometry used to describe the magnetic response. The internal magnetic field **H** is along the z axis and the total magnetization vector **M** precesses about this field. The quasistatic component of the precessing magnetization is shown as M_z and the vector **m** denotes the transverse $x-y$ plane dynamic magnetization response. The direction of the propagating MSW signal is indicated by the wave vector **k** along the y direction. The magnitude of **M** is taken to be constant and equal to the saturation magnetization M_s.

As discussed below, the precession is circular in the perpendicularly magnetized film MSFVW case and elliptical for in-plane magnetized films and the MSSW case. For the MSFVW case, M_z is constant. For the MSSW case, there is also a time dependent z component of **M** and M_z oscillates about its quasistatic, time-averaged value with a frequency of 2ω. Because of the rapid oscillations, this time-averaged value of M_z is taken as the effective static magnetization along the z axis.

In the experiment, the YIG film sample can have different orientations, relative to the precession diagram in Fig. 1. For MSFVW propagation, the z direction is perpendicular to the plane of the film. For MSSW signals, the z direction is in-plane. The applicable dispersion curves of MSW frequency ω_k vs wave number k for the MSFVW and MSSW cases are shown in Fig. 2. The curves were calculated from the well-known theoretical developments by Damon and Eshbach[10] for MSSW signals and Damon and van de Vaart[11] for MSFVW signals. The actual curves were calculated for the specific film properties and experimental conditions to be considered below. The thin film diagrams above the dispersion curves indicate the propagation configurations for the two cases.

Curve (a) in Fig. 2 is for MSFVW signals, with the film magnetized perpendicular to the film plane and propagation in-plane. The curve shown is for a static internal magnetic field H of 1929 Oe, a YIG saturation induction $4\pi M_s$ of 1750 G, and a gyromagnetic ratio γ of 2.8 GHz/kOe. The film thickness is 7.2 μm. Curve (b) is for MSSW signals, with the film magnetized in-plane and propagation perpendicular to this field and the magnetization direction. The specific curve shown is for a static internal magnetic field of 1114 Oe. Note that for these static internal field choices, the cut-off frequencies at low wave numbers are at 5.4 GHz for MSFVW signals and 5.0 GHz for MSSW signals, respectively. These values correspond to the experiments to be considered shortly.

The cut-off frequencies discussed above will be an important consideration for the development and results to follow. In the MSFVW case, this cutoff corresponds to the low frequency limit for the bulk spin wave band at zero wave number. This frequency limit is often written as[10]

$$\omega_H=\gamma H, \tag{1}$$

where γ denotes the gyromagnetic ratio for YIG and H denotes the applicable static internal magnetic field. In the MSSW case, the cutoff corresponds to the high frequency limit for the bulk spin wave band at zero k, given by

$$\omega_B=\gamma\sqrt{H(H+4\pi M_s)}. \tag{2}$$

Note that this upper limit frequency for bulk spin waves is the lower limit frequency for surface waves.[10] The frequencies ω_H and ω_B define the low frequency cut-off points for the MSFVW and MSSW transmission profiles at low power, respectively. Equation (1), with $H=1929$ Oe, yields $\omega_H=5.4$ GHz. Equation (2), with $H=1114$ Oe, yields $\omega_B=5.0$ GHz. These are the same cut-off points as shown in Fig. 2.

It is important to take note of the role of the saturation induction $4\pi M_s$ in determining these cut-off frequencies. In the MSFVW case, the cutoff comes from the ω_H expression of Eq. (1), and with $H=H_\perp-4\pi M_s$, where $H_\perp$ is the static external magnetic field applied perpendicular to the plane of the film. Note that a decrease in M_s will shift the MSFVW band edge *up* in frequency. In the MSSW case, the cutoff comes from the ω_B expression of Eq. (2), and with $H=H_\parallel$, where $H_\parallel$ is the static external magnetic field applied in the

plane of the film and perpendicular to the propagation direction. Here, a decrease in M_s will shift the MSSW band edge *down* in frequency.

The above discussion describes the situation at low power. Under low power conditions, the DMM amplitude is small, and the z component of the vector magnetization **M** is very close to M_s. This $M_z \cong M_s$ condition at low power is the basis of the band edge expressions given above. The critical point here is that, in general, it is M_z and not M_s which enters into the cut-off frequency relations at high power. Moreover, this M_z is related to the size of the dynamic response **m**. As already indicated, it is generally assumed that the magnitude of **M** is constant and equal to the saturation magnetization M_s. In this limit of fixed $|\mathbf{M}|$, it is clear from Fig. 1 that as the response becomes larger, M_z will decrease. To lowest order in $|\mathbf{m}|$, one would have

$$M_z = M_s - \frac{|\mathbf{m}|^2}{2M_s}. \tag{3}$$

It will prove convenient to consider the size of the M_z change with **m**, defined as

$$|\delta M_z| = \frac{|\mathbf{m}|^2}{2M_s}. \tag{4}$$

The decrease in M_z from M_s due to any increase in the response $|\mathbf{m}|$ will cause the same basic shifts in the band edges already described. This means that an increase in microwave power would be expected to shift MSFVW transmission profiles up and MSSW profiles down in frequency. The amount of these shifts, if they could be measured, would provide a direct determination of the DMM response $|\mathbf{m}|$ at a given power level. Note that $|\delta M_z|$ is strictly time independent for the MSFVW case and circular precession, and is explicitly defined as a time averaged quantity in the MSSW case with elliptical precession.

It will prove useful to have explicit expressions for these M_z dependent band edge frequencies. For the MSFVW geometry, with the static field perpendicular to the film plane, this power dependent low frequency band edge will be given by

$$\omega_{HF} = \gamma(H_\perp - 4\pi M_z). \tag{5}$$

Note that the field quantity inside the parentheses in Eq. (5) is simply the static internal field under high power and large precession amplitude conditions. In the small precession amplitude limit, for which $M_z = M_s$ is satisfied, ω_{HF} reduces to the cut-off frequency ω_H of Eq. (1). As the precession amplitude increases, the MSFVW frequency shift of the band edge is given by

$$\delta\omega_F = \omega_M \frac{|\delta M_z|}{M_s} = \frac{1}{2}\,\omega_M \frac{|\mathbf{m}|^2}{M_s^2}. \tag{6}$$

The ω_M parameter expresses the saturation induction in frequency units, according to $\omega_M = \gamma 4\pi M_s$. Note that the frequency shift is positive. This means that with increasing power, the MSFVW band edge frequency is shifted towards higher frequency.

For the MSSW geometry, with the static field in-plane, the corresponding cut-off frequency is given by

$$\omega_{BS} = \gamma\sqrt{H_\parallel(H_\parallel + 4\pi M_z)}. \tag{7}$$

Recall that in the MSSW case, with the static field in-plane and in-plane demagnetizing factors taken to be zero, the static internal field $H_\parallel$ and the static internal field H are identical. In the small precession amplitude limit in which $M_z = M_s$ is satisfied, ω_{BS} reduces to the usual low power cut-off frequency in the limit of zero wave number, ω_B. As the precession amplitude increases, the frequency shift of the band edge from ω_B, to lowest order in $|\mathbf{m}|$, is given by

$$\delta\omega_S = -\frac{1}{2}\frac{\omega_H\omega_M}{\omega_B}\frac{|\delta M_z|}{M_s} = -\frac{1}{4}\frac{\omega_H\omega_M}{\omega_B}\frac{|\mathbf{m}|^2}{M_s^2}. \tag{8}$$

The negative sign for the middle section and the right-hand side of Eq. (8) indicates that the MSSW band edge frequency is shifted towards lower frequency.

For simplicity, the contributions of various anisotropy terms to the effective fields and band edge expressions have been neglected. The effective fields in YIG due to anisotropy are in the range of 50 Oe. These anisotropy fields will introduce some small discrepancies between the actual static external fields used in the experiments and the theoretical field values used in the above calculations to position the band edges at 5 GHz. These small discrepancies are not important to the frequency shift analysis.

It is clear from Eqs. (6) and (8) that the decrease in M_z which accompanies any increase in the DMM amplitude produces a shift in the applicable magnetostatic wave band edge frequency and also shifts the transmission profile tied to that band edge. The connection between these shifts and the DMM amplitudes can be obtained in a relatively simple form by introducing a reduced amplitude function $u(y)$. For MSFVW signals in a perpendicular magnetized film and a precession which is nearly circular, one may write the real dynamic magnetization response as

$$\mathbf{m}_F(y,t) = \mathrm{Re}\{\sqrt{2}M_s u_F(y)(\mathbf{x} - i\mathbf{y})e^{i(\omega_k t - ky)}\}, \tag{9}$$

where $\mathbf{m}_F(y,t)$ denotes the transverse $x-y$ component dynamic magnetization response for the propagating MSFVW signal, $u_F(y)$ is a complex MSFVW amplitude function, **x** and **y** denote x and y direction unit vectors, k is the wave number for y direction propagation, and ω_k is the signal frequency. Note that the precession sense for this MSFVW signal is Larmor, the polarization is circular, and the dynamic magnetization amplitude for the circularly polarized response is given by

$$|\mathbf{m}_F(y,t)| = \sqrt{2}M_s|u_F(y)|. \tag{10}$$

From Eqs. (1), (6), and (10), a dynamic response in the $|\mathbf{m}_F|/M_s = 3\%-5\%$ range corresponds to $|u_F| \cong 0.021-0.035$ and $M_z/M_s = 0.99955-0.99875$. While the changes in M_z from M_s are clearly small at these amplitudes, the corresponding frequency shifts turn out to be significant.

In general, the complex function $u(y)$ describes the envelope of the MSW wave packet which is generated and propagated in the particular experiment of interest. If $|u(y)| \ll 1$ is satisfied, one would have linear MSW wave packets of small amplitude. Larger values of $|u(y)|$ could

correspond, for example, to MSW solitons of the sort discussed in Refs. 1–6. In cw experiments or for rectangular pulses of long duration, $u(y)$ would be more-or-less constant over the duration of the pulse. High power cw excitation can lead to spin wave instability effects, the onset of auto-oscillation, or chaos. These special nonlinear effects are not considered here.

In the MSSW case, with the film magnetized in-plane, the precession will generally be elliptical. If it is assumed that the polarization is the same as for low power ferromagnetic resonance in the $k=0$, $\omega=\omega_B$ limit, the precession response may be written according to

$$\mathbf{m}_S(y,t)=\mathrm{Re}\left\{\sqrt{2}M_s u_S(y)\left(\frac{\omega_H}{\omega_B}\mathbf{x}-i\mathbf{y}\right)e^{i(\omega_k t-ky)}\right\}, \quad (11)$$

where $u_S(y)$ is a complex MSSW amplitude response function. The ω_H and ω_B parameters in Eq. (11) are the same frequency parameters as defined above, subject to the $H=H_{\|}$ condition applicable to the MSSW geometry. The precession sense for this MSSW signal is also Larmor. The polarization is elliptical, with the major axis along the y direction and in the plane of the film. The minor axis of the precession ellipse is along the x direction and normal to the film plane. In the MSSW case, one obtains a *time-averaged* dynamic magnetization amplitude for the elliptically polarized response given by

$$|\mathbf{m}_s(y,t)|=\sqrt{1+\omega_H^2/\omega_B^2}M_s|u_S(y)|. \quad (12)$$

Equations (10) and (12) relate the $|\mathbf{m}|$ responses to the $u(y)$ functions for the MSFVW and MSSW cases, respectively. These equations may be used in Eqs. (6) and (8), respectively, to obtain explicit frequency shift connections with the $u(y)$ responses. These connections are strictly valid only in the $k\rightarrow 0$ limits corresponding to ferromagnetic resonance. These results are applicable, therefore, only for a signal frequency ω_k which is close to ω_H in the MSFVW case, or close to ω_B in the MSSW case.

Now define a frequency response coefficient N, according to

$$\delta\omega=N|u|^2, \quad (13)$$

where $|u|^2$ denotes the square of the magnitude of the appropriate $u(y)$ function defined above. The quantity $|u|^2$ represents a normalized power response for the MSW signal which scales, more-or-less, with input power. For convenience, $|u|^2$ will be termed *power amplitude*.[3,6]

Based on the above, one may immediately write down N parameters for the MSFVW and MSSW cases. The results are

$$N_F=\omega_M \quad (14)$$

and

$$N_S=-\frac{\omega_M\omega_H}{4\omega_B}\left(1+\frac{\omega_H^2}{\omega_B^2}\right), \quad (15)$$

respectively. For YIG under the specific conditions used above, namely $4\pi M_s=1750$ G, $H=1929$ Oe for the MSFVW case, and $H=1114$ Oe for the MSSW case, one obtains $N_F=4.9$ GHz and $N_S=-1.1$ GHz. These frequency shift scale parameters will be important for the experiment and the data presentation to follow. In order to make contact with previous work, the data will be presented in terms of the power amplitude $|u|^2$ rather than actual frequency shift.

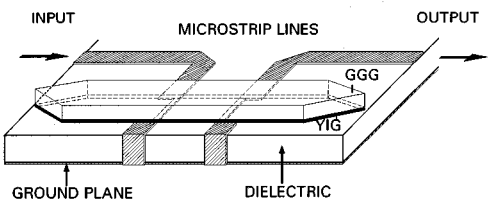

FIG. 3. Diagram showing the yttrium iron garnet (YIG) film and the YIG film transducer structure used for the experiments. The structure consists of two planar 50 Ω microstrip transmission lines which narrow down to 50-μm-wide input and output transducer sections. The long and narrow YIG film on a gadolinium gallium garnet (GGG) substrate is positioned YIG side down over the transducer sections of the input and output microstrip lines. The ends of the YIG film are tapered.

The physical significance of the above frequency shift scale values is twofold. First, DMM responses with $|\mathbf{m}|/M_s$ in the 1% range and $|u|^2$ in the range of 10^{-4} yield frequency shifts on the order of MHz. Second, based on the $u(y)$ connections used here, the frequency shift response is about a factor of 5 smaller for MSSW signals than for MSFVW signals. Both effects are borne out experimentally. The N parameter defined above is the same as the so-called nonlinear response parameter used by Zvezdin and Popkov[1] and others[3–6,8] in the analysis of nonlinear MSW pulse propagation and soliton formations, based on the nonlinear Schrödinger equation.

III. FREQUENCY SHIFT MEASUREMENTS

The experiments were carried out with a 7.2-μm-thick single-crystal YIG film sample of dimensions 15×2.5 mm. The film was grown on a (111) plane single-crystal gadolinium gallium garnet substrate by the method of liquid phase epitaxy.[12] The film has slightly pinned surface spins, evident from the relatively small but distinct notches observed in the MSW transmission loss vs frequency curves for both forward volume waves and surface waves. These notches are due to dipole-exchange gap effects[12,13] and are generally more pronounced for MSFVW excitations than for surface waves. Figure 3 shows the transducer structure used to excite magnetostatic waves in the film. Standard 50 Ω input and output microstrip lines narrow to 50-μm-wide, 2.5-mm-long transducers under the YIG film. These lines are on the top surface of a RT/duroid® laminate dielectric substrate with a conducting ground plane backing. The separation between the input and output transducer lines was 4 mm. As indicated in Fig. 3, the ends of the 2.5×15 mm YIG strip were tapered in order to reduce unwanted reflections. The sample was positioned with the center section of the strip over the transducers.

The basic experiment consisted of applying microwave power to the input transducer while sweeping the input frequency over some range which was wide enough to pick up particular features in the detected transmission profile at the output transducer. It was then possible to follow the fre-

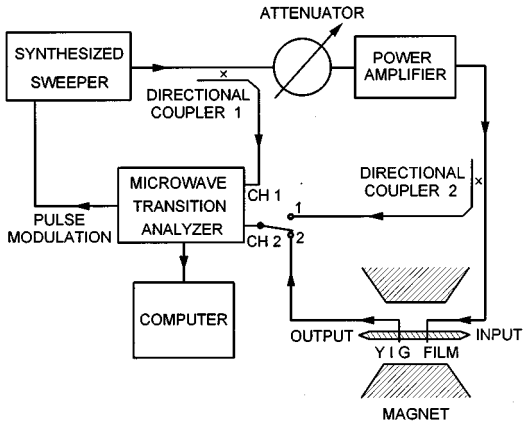

FIG. 4. Block diagram of the microwave measurement system.

quency shift for one or more of these features as a function of input power. These shifts were then used to determine the power amplitude parameter $|u|^2$ as a function of input power.

A block diagram of the measurement setup is shown in Fig. 4. A microwave synthesized sweeper provides microwave power to the input transducer and the YIG film through an attenuator and power amplifier. The YIG film is positioned in the gap of an electromagnet which provides the static external magnetic field. The output transducer signal is analyzed with a microwave transition analyzer (MTA). Directional couplers provide reference signals to the MTA as well. The key instrument in the setup is the HP71500A microwave transmission analyzer. The MTA controls the frequency of the microwave synthesized sweeper and also provides a pulse modulation to the signal.

Overall transmission profiles at low power are obtained in the usual way, by sweeping the frequency over the entire MSW pass band and measuring output power vs frequency. Representative data of this sort are shown in Fig. 5 for the MSSW configuration discussed above. The input power was 0.5 mW. The MSSW pass band between 5.0 and 5.6 GHz is clearly evident, as is the band edge cutoff at a frequency

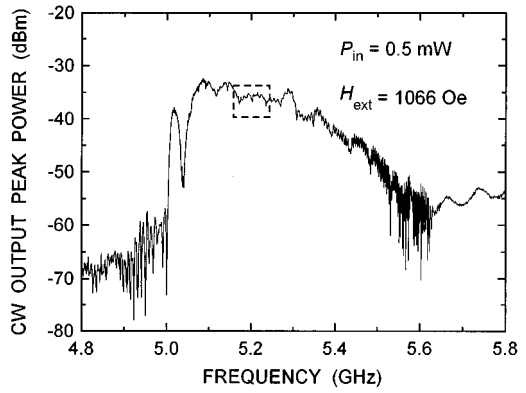

FIG. 5. Low power cw transmission vs frequency profile for the surface wave configuration, with an in-plane static external magnetic field of 1066 Oe and propagation perpendicular to the field direction. The input power was 0.5 mW. The dashed rectangle marks the operating frequency interval for the frequency shift measurements at high power.

close to 5 GHz. The gradual decrease in output power from the low to the high frequency end of the pass band is due to the shape of the ω_k vs k dispersion curve (b) in Fig. 2, with a slope $d\omega_k/dk$ and corresponding group velocity which decrease with increasing frequency. In the present situation, the propagation time at 5.6 GHz is sufficiently long to cause a significant decay in the output signal level due to relaxation, so that the detected output power merges into the background power above about 5.6 GHz. These considerations are discussed at length in Refs. 1 and 4.

Apart from the general shape of the transmission profile shown in Fig. 5, it is important to observe that the profile itself contains numerous small features in the form of dips and notches. Some of these small features are related to special aspects of the dispersion curves not shown in Fig. 2 which relate to pinning effects, dipole exchange gaps, and other dispersion properties for which a complete discussion is beyond the scope of this article. The main point for this work is that these features decorate the transmission profile in a way which represents intrinsic properties and are tied to the band edge in a definite and reproducible manner. The operational assumption here is that a frequency shift for one or more of these features has the same significance as a frequency shift for the band edge. The results presented below will be based on the measured frequency shifts for these features, both for MSFVW signals and for MSSW signals.

Several such small but distinct features on the profile in Fig. 5, located near 5.2 GHz, are highlighted by the rectangular, dashed line box near the middle of the figure. As will be evident shortly, these features are found to shift down in frequency in a systematic manner as the input power is increased. It will be these shifts which are the basis of the DMM response determinations reported here.

It is a relatively easy matter to measure accurate transmission profiles, such as the one shown in Fig. 5, at low power. It is much more difficult to obtain such curves at high power, due primarily to heating effects. A small rise in temperature results in a decrease in the saturation magnetization M_s. Because of the small changes in M_z which are involved in the nonlinear shifts of interest here, such thermal effects can completely mask the frequency shifts due to the DMM response. For actual frequency shift measurements, it was necessary to pay careful attention to heating effects. Such effects were eliminated by operating the MTA network analyzer in the pulsed mode instead of the standard cw mode. In this mode, profiles like the one shown in Fig. 5 were obtained by changing the frequency in small steps and making a series of pulse measurements at each frequency. Pulse widths down to 1 μs and pulse repetition rates down to 1 kHz were used. The corresponding duty cycles, 0.1% or so, were needed to avoid heating effects. It is important to keep in mind the fact that the features in the transmission profiles which are used to track the frequency shifts are generally small. The frequency shifts, while measurable, are also small. Accurate and reproducible measurements in experiments such as these require careful attention to heating effects and the resulting changes in M_s with temperature. The duty cycles cited above were determined experimentally, and were well below those which lead to shifts due to heating.

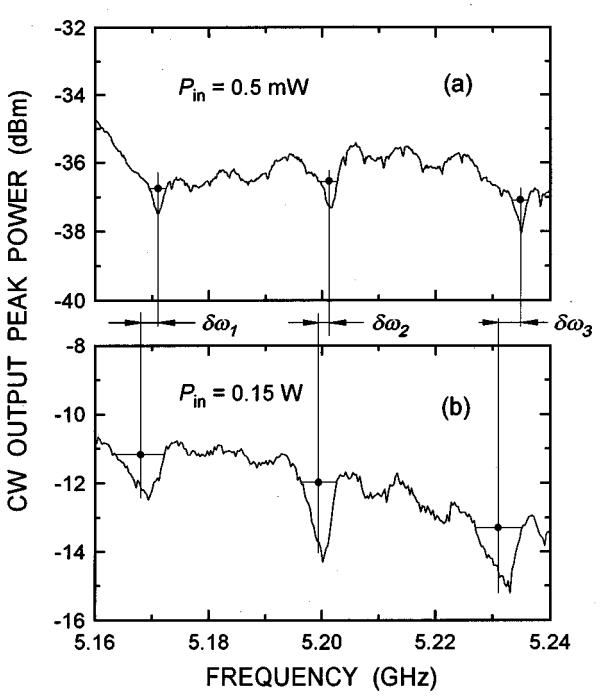

FIG. 6. Expanded view of the dashed rectangle transmission profile region in Fig. 5. Trace (a) is for an input power of 0.5 mW, the same as in Fig. 5. Trace (b) is for an input power of 0.15 W. The dots and the vertical lines centered on the three dip features in each trace are intended as a guide to the eye in determining the frequency shifts from low to high power. These shifts are indicated by the $\delta\omega_1$, $\delta\omega_2$, and $\delta\omega_3$ labels in the space between the two profile segments.

The actual measurements of frequency shift vs input power were based on the observation of small segments of the MSW transmission profiles. Figure 6 shows one such segment which corresponds to the profile section shown in the dashed line box in Fig. 5. The basic displays are the same as in Fig. 5, and show the output power in dBm as a function of frequency. Note the expanded frequency scale, with 10 MHz per small horizontal scale division. The upper profile section in Fig. 6(a) was obtained at a low power of 0.5 mW, as before. The lower profile section in Fig. 6(b) was obtained at a relatively high power of 0.15 W.

On the expanded scale of Fig. 6, the specific notch features which are the basis of the frequency shift measurement are clearly evident. Both profile segments show three distinct dips, presumably related to dipole exchange gaps in the actual dispersion curves for films with a small amount of surface spin pinning. The detailed origins of these features are not particularly important here. The point of importance is that these dips shift down in frequency as the power is increased. These shifts are readily apparent from the profile segments. The dots and the vertical lines in the figure are intended as a guide to the eye in following these shifts, labeled in the figure as $\delta\omega_1$, $\delta\omega_2$, and $\delta\omega_3$. Note that these shifts are to lower frequencies and are on the order of 2–4 MHz.

In addition to the frequency shifts due to power, several other points of comparison between the low and high power profile segments in Fig. 6 are in order. First, note that the increase of the input power from 0.5 mW to 0.15 W represents an increase of about 25 dB. The increase in the overall output power levels from Figs. 6(a) to 6(b) is also by about 25 dB. Second, take note of the change in the shape of the dipole-exchange dips from low to high power. The dips tend to be wider, deeper, and more asymmetric at the high power, with shapes which are steeper on the high frequency side. This change in shape can be attributed to the power dependent frequency shift, even within a single dip. Since the shift should be smaller at lower powers, the actual dip minima points in frequency will be somewhat higher than the frequency midpoint at the base of the dip. While this effect is small, on the order of 1–2 MHz for the dips in Fig. 6, it is significant enough to introduce errors into quantitative frequency shift vs power determinations and the corresponding calibration of the power amplitude response. For this reason, it is important that the position of a given dip at a given power should be determined at the base of the dip and not at the sharp minimum. The solid dots in Fig. 6 denote these center frequency points for the dips shown.

Ideally, one would expect to see the same exact shifts for all features. As the data in Fig. 6 indicate, this ideal situation is not realized experimentally. Even though, in the MSSW case now under discussion, there is consistent shift in the dip positions toward lower frequencies, the shift amounts vary by a factor of 2 or so. For the present series of measurements for both the MSSW and MSFVW configurations, estimates of the basic nonlinear shifts were obtained as the average over the observed base center frequency for three or more notches. The data in Fig. 6 actually show a worst case situation. Generally, the spreads in frequency shift values were smaller than apparent here.

The cw profile and the limited sweep short profile measurements shown in Figs. 5 and 6 for the MSSW configuration are more-or-less typical of all the raw data for both the MSFVW and the MSSW configurations. Except that the frequency shifts at high power for the MSFVW configuration were to higher frequency as one would expect, and were generally larger than the MSSW shifts. The dipole-exchange notches in the MSFVW were generally more pronounced, and the individual shift values were closer together.

In closing this section on the nonlinear frequency shift measurements, it is important to make several points. First, it is important to note that reliable frequency shift measurements made directly on the band edge are not possible. Due to a variety of effects, which include the occurrence of ferromagnetic resonance at the frequency corresponding to the band edge, the shape of the transmission profile just at the band edge is complicated. This is evident from the shape of the band edge transmission profile near 5 GHz in Fig. 5. The accurately measurable frequency of the sharp onset of magnetostatic backward volume waves is practically constant with power. This band edge problem leads to the second point. The present technique is applicable only for situations in which the MSW transmission vs frequency profile contains distinct features which are reasonably close to the band edge and which can be accurately tracked as a function of power. It was not possible, for example, to use this technique to measure the DMM response for magnetostatic backward volume wave signals. For these signals, there are no higher-

order dispersion branches which cross the main branch, and no corresponding dipole-exchange gap effects to produce dips in the transmission profiles exist for this type of magnetostatic wave.

IV. DMM POWER AMPLITUDE

Frequency shift measurements as a function of input power for the MSFVW and MSSW configurations were made as described above and used to determine values of the DMM power amplitude parameter $|u|^2$ vs input power level according to the analysis given in Sec. II. The following quantities were measured for each experimental point: the average input power within the relevant narrow frequency sweep interval, the average frequency shift for the selected features, the standard deviation for those shifts, and the average output power over the sweep. These measurements were made for input power levels from 0 to 4 W in both MSFVW and MSSW configurations.

Note that the profiles in Figs. 5 and 6 correspond to power measurements at the output transducer. The observed frequency shift features, however, reflect the effect of the DMM power amplitude on δM_z over the entire propagation path from input to output. Hence, the $|u|^2$ values obtained from the frequency shift measurements and Eqs. (13) and (14), or (13) and (15), will correspond to some average power amplitude. The $|u|^2$ response can change along the propagation path for a variety of reasons. First, decay due to damping is always present, both in the linear and in the nonlinear response regimes. Second, there are the nonclassical nonlinear effects which lead to well known spin wave instability, auto-oscillation, and chaotic phenomena. Such effects are considered briefly in the discussion below.

A. Results for MSFVW signals

The results of the measurements for the MSFVW configuration are shown in Fig. 7. The ω_H band edge was set at 5.4 GHz in this case. The required perpendicular-to-plane external field was 3744 Oe. The narrow operational frequency interval for the frequency shift measurements was around 5.6 GHz, from 5.55 to 5.65 GHz. Figure 7(a) shows the results for the MSFVW power amplitude as a function of the input microwave power. It is important to keep in mind that the vertical axis, although expressed in terms of the power amplitude $|u|^2$ response, actually represents frequency shift data for the transmission profile features already discussed. The scale factor is $+4.9$ GHz per $|u|^2$. At the limit of the vertical axis scale, with $|u|^2=50\times10^{-4}$, the actual data would correspond to a frequency shift of 24.5 MHz. Figure 7(b) shows output power vs input power. In both graphs, the solid dots represent the data. The solid lines through the points are intended as a guide to the eye only.

Figure 7(a) shows an almost linear increase in the output power amplitude $|u|^2$ with input power for low power. For input powers above 0.5 W or so, the response falls off and suggests the onset of some sort of saturation at high power. The slope of the near linear low power response for $|u|^2\times10^4$ vs input power is approximately 40 W^{-1}. The largest value of $|u|^2\times10^4$, at an input power of 4 W, is 45. This corresponds to a $4\pi|\mathbf{m}|$ value of 166 G, or about 10% of the

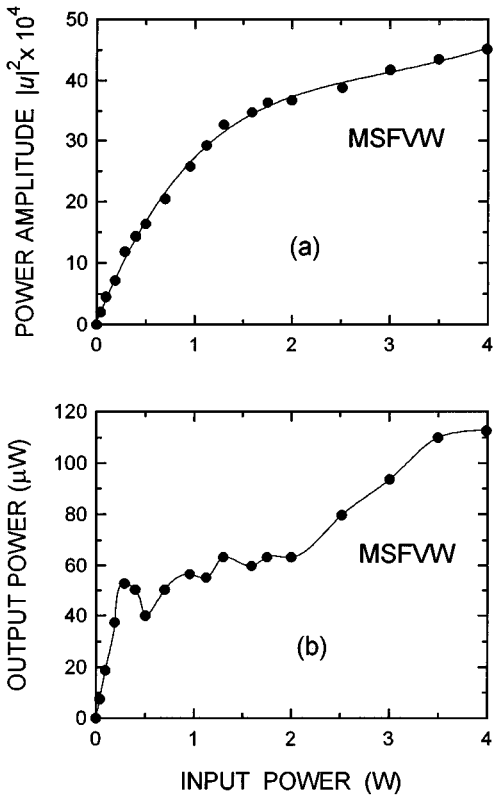

FIG. 7. Measurement results on (a) power amplitude and (b) output power as a function of input power for MSFVW signals. The measurement frequency interval was 5.55–5.65 GHz and the perpendicular-to-film external magnetic field was 3744 Oe.

YIG saturation induction. Such a response would be expected to be in a nonlinear regime, consistent with the trend of the data.

Turn now to the power response in Fig. 7(b). The output power vs input power dependence in Fig. 7(b) undergoes a rather rapid increase for input powers up to about 0.3 W, followed by an irregular and slowly increasing response for powers up to 2 W, and then a somewhat more rapid up to 4 W. The output power vs input power response profile in Fig. 7(b) has a very different character from the $|u|^2$ response in Fig. 7(a). One does have the nonlinear onset in the same range of input powers, 0.3–0.5 W. Other than this, however, the profiles are completely different. The initial output vs input power response in Fig. 7(b), approximately 240 μW/W, is of the same order as the 130 μW/W response found for the MSFVW solitons in Ref. 6. In the soliton case, however, the output power rises above the linear response at high power. Here, for near cw signals, one finds a saturation of sorts. These data show that the connection between the MSFVW amplitude response and output power is complicated.

Part of these complications, as already indicated, has to do with the fact that the $|u|^2$ response obtained from the frequency shift for output profile features must represent some sort of average over the propagation path from input to output. The effect of propagation loss due to damping may be readily estimated for MSFVW signals, based on the relaxation rate and group velocity parameters from Ref. 6,

5.6×10^6 rad/s and 4.57×10^6 cm/s, respectively. These values yield a decay in $|u|^2$ from input to output, over the 4 mm separation between transducers, by a factor of 2.7. This means that for $|u|^2$ values at input, the $|u|^2$ values in Fig. 7(a) should be multiplied by some factor between 1 and 2.7. The factor of 1 applies if the frequency shifts are dominated by the response at input. The factor of 2.7 applies if the dominant effect is at output. The actual scaling, of course, is likely to be somewhere in between.

The initial $|u|^2\times10^4$ vs input power response of 40 W^{-1} noted above may be compared with other results. The corresponding response for 10 ns wide pulse MSFVW signals in Ref. 6 was estimated at 2.2 W^{-1}, down by a factor of 20–60 or so from the present cw result, depending on the averaging effects of decay as just discussed. It is certainly reasonable to expect a larger response for long pulse signals than for short pulses. It is also possible to estimate the response from theory.[7,14] With parameters applicable to the MSFVW situation under consideration here, and under the assumption of 100% transfer of the input energy to the propagating MSW signal, the estimated $|u|^2\times10^4$ vs input power linear response at the input transducer is about 200 W^{-1}. This compares favorably to the 40–120 W^{-1} values implied from the low power response data in Fig. 7(a) with propagation loss due to damping taken into account.

It is also important to note the importance of nonclassical nonlinear effects. Estimates of the $|u|^2$ response needed for the onset of second order spin wave instability processes under conditions of uniform mode ferromagnetic resonance at 5.4 GHz in perpendicular-to-plane magnetized YIG films are well below the values shown in Fig. 7(a). This means that such processes must play a key role in the nonlinear responses found in both Figs. 7(a) and 7(b). A relevant discussion of second order spin wave instability processes in YIG films may be found in Ref. 15 and references cited therein. A comprehensive treatment of these considerations is beyond the scope of this experimental report on a frequency shift measurement technique to access the DMM response in films.

B. Results for MSSW signals

The corresponding MSSW results are shown in Fig. 8. Here, the ω_B band edge was set at 5.0 GHz and the required external in-plane field was 1066 Oe. The narrow operational frequency interval for the shift measurements was around 5.2 GHz. Figure 8(a) shows the results on the calculated MSSW power amplitude vs input power. As for Fig. 7(a), it is important to keep in mind that the vertical axis, although expressed in terms of the power amplitude $|u|^2$ response, represents frequency shift data for the transmission profile features already discussed. The MSSW scale factor is -1.1 GHz per $|u|^2$. At the limit of the vertical axis scale, with $|u|^2=60\times10^{-4}$, the actual data would correspond to a measured frequency shift of -6.6 MHz. Figure 8(b) shows output power vs input power. The format is the same as for Fig. 7.

The MSSW results are somewhat different from the MSFVW results in Fig. 7. The key differences are in (1) the very rapid initial responses and saturation at low power for both

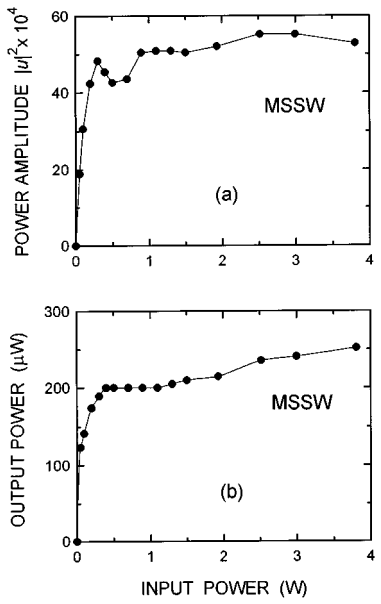

FIG. 8. Measurement results on (a) power amplitude and (b) output power as a function of input power for MSSW signals. The measurement frequency interval was 5.16–5.24 GHz and the in-plane external magnetic field was 1066 Oe.

the power amplitude and output power determinations and (2) the fact that the power amplitude vs input power and the output power vs input power responses in Figs. 8(a) and 8(b) track each other rather well. The slope of the initial power amplitude response, although difficult to estimate because of the very rapid increase, has a lower limit of about 1000 W^{-1}. Saturation clearly occurs for input powers above 0.5 W or so.

As for the MSFVW results, several points of comparison are in order. Consider first the rapid initial power amplitude response. This response is significantly bigger than the 7.5 W^{-1} value obtained from the magnetostatic backward volume wave (MSBVW) soliton experiments of Ref. 3 for in-plane magnetized YIG films at about the same frequency. Here, there are two factors to consider and both support a bigger response in the MSSW case: (1) The coupling between the transducer and dynamic magnetization is stronger for MSSW signals compared to MSBVW signals. (2) As in the MSFVW comparison, 1 μs long pulse signals are expected to show a bigger response relative to short pulse signals in the 10 ns range.

The input power level for the onset of saturation effects appears to be about the same for the MSSW case as for the MSFVW case, 0.5 W or so. The saturation values of 50–60 for $|u|^2\times10^4$ correspond to $4\pi|\mathbf{m}|$ in a range of 146–160 G, also on the order of 10% of the YIG saturation induction. These saturation effects on both $|u|^2$ and output power are likely due to second order spin wave instability processes, the same as for MSFVW signals. Even though the YIG film is magnetized in-plane in the MSSW case, and the 5.2 GHz operating point is near the top of the spin wave band at low wave number, the bottom of the spin wave band is at 3 GHz and still well above the half-frequency point of 2.6 GHz which would be required for first order processes. Moreover,

strip line coupling considerations are approximately the same for the MSSW as for MSFVW signals.

The same basic remarks concerning propagation decay due to damping and averaging effects, made in the MSFVW discussion above, apply here as well. As evident from the slopes of the dispersion curves in Fig. 2, the MSSW group velocity at an operating point of 5.2 GHz will be somewhat smaller than the corresponding MSFVW group velocity at 5.6 GHz. This means that the decay in $|u|^2$ from input to output due to damping alone will be even more significant than before. The $|u|^2$ results in Fig. 8(a), as in Fig. 7(a), represent an average effect over the propagation length of the device structure.

V. SUMMARY AND CONCLUSION

This work has described a technique to use frequency shift measurements for specific features in the transmitted power vs frequency profiles for magnetostatic wave signals in YIG films as a function of power to determine the dynamic microwave magnetization response for the MSW signal. The technique has been applied to cw magnetostatic forward volume wave signals and magnetostatic surface wave signals propagated in a YIG film delay line structure at 5–6 GHz. The data give response parameters which are consistent with previous pulse experiments and theory. Moreover, the detailed results show that the observed DMM response is affected by many factors, including averaging effects over the propagation path for the signal and nonclassical nonlinear effects such as second order spin wave instability processes. The technique allows empirical access to this important response parameter.

ACKNOWLEDGMENTS

The authors thank Dr. I. Laulicht, Dr. P. Kabos, Dr. B. A. Kalinikos, and Dr. D. D. Stancil for helpful discussions. The films were provided by Dr. J. D. Adam, Westinghouse Science and Technology Center, Pittsburgh, Pennsylvania. This work was supported in part by the National Science Foundation, Grant Nos. DMR-8921761 and DMR-9400276, and the U.S. Army Research Office, Grant Nos. DAAL03-91-G-0327 and DAAH04-95-1-0325.

[1] A. K. Zvezdin and A. F. Popkov, Zh. Eksp. Teor. Fiz. **84**, 606 (1983) [Sov. Phys. JETP **57**, 350 (1983)].
[2] B. A. Kalinikos, N. G. Kovshikov, and A. N. Slavin, Pis'ma Zh. Eksp. Teor. Fiz. **38**, 343 (1983) [JETP Lett. **38**, 413 (1983)].
[3] M. Chen, M. A. Tsankov, J. M. Nash, and C. E. Patton, Phys. Rev. B **49**, 12773 (1994).
[4] M. Chen, J. M. Nash, and C. E. Patton, J. Appl. Phys. **73**, 3906 (1993).
[5] A. N. Slavin and G. M. Dudko, J. Magn. Magn. Mater. **86**, 115 (1990).
[6] M. A. Tsankov, M. Chen, and C. E. Patton, J. Appl. Phys. **76**, 4274 (1994).
[7] V. F. Dmitriev and B. A. Kalinikos, Izv. Vyssh. Uchebn. Zaved. Fiz. **31**, 24 (1988) [Sov. Phys. J. **31**, 875 (1988)].
[8] B. A. Kalinikos, N. G. Kovshikov, and A. N. Slavin, J. Appl. Phys. **69**, 5712 (1991).
[9] K. Gnatzig, M. Dötsch, M. Ye, and A. Brockmeyer, J. Appl. Phys. **62**, 4839 (1987).
[10] R. W. Damon and J. R. Eshbach, J. Phys. Chem. Solids **19**, 308 (1961).
[11] R. W. Damon and H. van de Vaart, J. Appl. Phys. **36**, 3453 (1965).
[12] J. D. Adam, M. R. Daniel, P. R. Emtage, and S. H. Talisa, in *Physics of Thin Films*, edited by M. H. Francombe and J. L. Vossen (Academic, Boston, 1991), Vol. 15, p. 2, and references therein.
[13] J. D. Adam, T. W. O'Keeffe, and R. W. Patterson, J. Appl. Phys. **50**, 2446 (1979).
[14] D. D. Stancil, *Theory of Magnetostatic Waves* (Springer, New York, 1993), p. 200.
[15] Y. T. Zhang, C. E. Patton, and G. Srinivasan, J. Appl. Phys. **63**, 5433 (1988).